frontiers in Physics

ORIGINAL RESEARCH
published: 23 July 2020
doi: 10.3389/fphy.2020.00173

A Constitutive Model for Cemented Tailings Backfill Under Uniaxial Compression

Bingbing Tu[1,2], *Lang Liu*[3,4]*, *Kangli Cheng*[3], *Bo Zhang*[3], *Yujiao Zhao*[3], *Qixing Yang*[3] and *Kiil Song*[5]

[1] College of Science, Xi'an University of Science and Technology, Xi'an, China, [2] State Key Laboratory of Green Building in Western China, Xi'an University of Architecture and Technology, Xi'an, China, [3] Energy School, Xi'an University of Science and Technology, Xi'an, China, [4] Key Laboratory of Western Mines and Hazards Prevention, Ministry of Education of China, Xi'an, China, [5] Department of Civil Engineering, Inha University, Incheon, South Korea

Constitutive model is the foundation describing the mechanical properties of materials. Cemented tailings backfill (CTB) plays an important role in goaf filling. However, a universally applicable constitutive model for CTB has not been proposed yet. In this paper, a two-stage constitutive model of CTB under uniaxial compression was established, based on the Weibull distribution density function, the strain equivalence principle and the damage mechanics theory. Eight groups of CTB samples with a diameter of 50 mm and a height of 100 mm prepared with different solid contents (70–78 wt%) and cement-sand ratios (1/4–1/10) were subjected to uniaxial compression tests to verify the validity of the theoretical model. The compared results showed that the predictions of the proposed constitutive model agreed well with the experimental results. The following conclusions were also obtained: (i) Solid content and cement-sand ratio had a significant effect on the basic mechanical parameters of the CTB samples, especially at the peak stress; (ii) The constitutive model of CTB was similar to that of the ordinary cement mortar M5, but with obvious residual stress; (iii) The failure mode of the CTB specimens under uniaxial compression was mainly tensile failure. The results presented in this paper contribute to a better understanding of the uniaxial compression characteristics of CTB and lay an important foundation for future research.

Keywords: cemented tailings backfill, constitutive model, strain equivalence principle, Weibull distribution, uniaxial compression strength

OPEN ACCESS

Edited by:
Longjun Dong,
Central South University, China

Reviewed by:
Jordan Yankov Hristov,
University of Chemical Technology and Metallurgy, Bulgaria
Laurent Olivier Louis,
New England Research, United States

***Correspondence:**
Lang Liu
liulang@xust.edu.cn

Specialty section:
This article was submitted to Interdisciplinary Physics, a section of the journal Frontiers in Physics

Received: *03 March 2020*
Accepted: *24 April 2020*
Published: *23 July 2020*

Citation:
Tu B, Liu L, Cheng K, Zhang B, Zhao Y, Yang Q and Song K (2020) A Constitutive Model for Cemented Tailings Backfill Under Uniaxial Compression. Front. Phys. 8:173. doi: 10.3389/fphy.2020.00173

HIGHLIGHTS

- A constitutive model for CTB under uniaxial compression was established.
- Influences of solid content and cement-sand ratio were analyzed.
- The failure mode of CTB specimens under uniaxial compression was mainly tensile failure.

INTRODUCTION

As one of the most commonly used filling aggregates for goaf filling, cemented tailings backfill (CTB) plays an important role in the safe, green, and efficient mining of metals [1]. CTB can effectively solve the problems related to deep rock pressure control and surface subsidence above the goaf, and can also avoid the environmental pollution caused by the accumulation of tailings

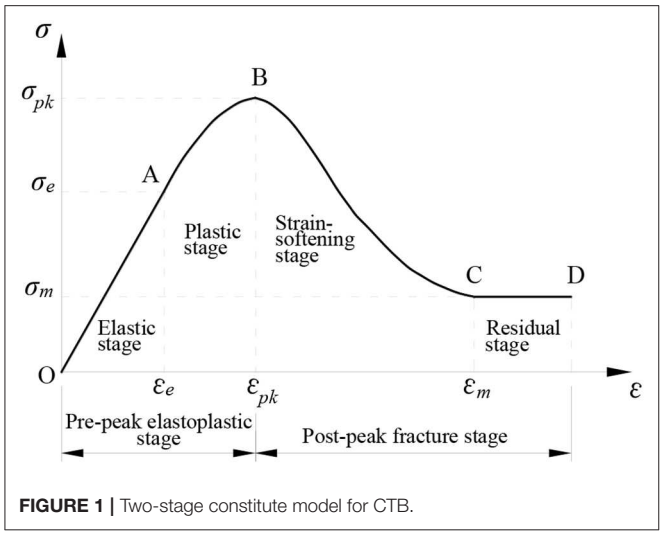

FIGURE 1 | Two-stage constitute model for CTB.

In this paper, the elastic modulus E of the CTB is defined as follows, considering the influence of solid content and cement-sand ratio.

$$E = E(x_1, x_2), \tag{9}$$

where x_1 is the solid content, and x_2 is the cement-sand ratio.

Then, Equation (8) can be rewritten as:

$$\sigma = \begin{cases} E(x_1,x_2)\varepsilon \exp[-(\frac{\varepsilon}{F_0})^m], \varepsilon < \varepsilon_m \\ E(x_1,x_2)\varepsilon_m \exp[-(\frac{\varepsilon_m}{F_0})^m], \varepsilon \geq \varepsilon_m \end{cases}. \tag{10}$$

The corresponding constitutive model is shown in **Figure 1**, where σ_e, $\sigma_{pk,}$ and σ_m represent the elastic stress, the peak stress, and the residual stress, and the corresponding strains ε_e, $\varepsilon_{pk,}$ and ε_m are the elastic strain, the peak strain, and the starting strain of the residual stage, respectively.

DETERMINATION OF MODEL PARAMETERS

To determine the unknown parameters m and F_0 in the first formula of Equation (10), the following boundary conditions are given:

(i) $\sigma = \sigma_{pk}, \varepsilon = \varepsilon_{pk}$, (ii) $\varepsilon = \varepsilon_{pk}, d\sigma/d\varepsilon = 0$.

Based on the given boundary conditions (i), the following equation can be obtained:

$$E(x_1,x_2)\varepsilon_{pk} \exp[-(\frac{\varepsilon_{pk}}{F_0})^m] = \sigma_{pk}. \tag{11}$$

Then, according to the boundary conditions (ii), the following equation can be obtained:

$$\frac{d\sigma}{d\varepsilon} = E(x_1,x_2)[1 - m(\frac{\varepsilon}{F_0})^m] \exp[-(\frac{\varepsilon}{F_0})^m], \tag{12}$$

$$E(x_1,x_2)[1 - m(\frac{\varepsilon_{pk}}{F_0})^m] \exp[-(\frac{\varepsilon_{pk}}{F_0})^m] = 0, \tag{13}$$

where $E(x_1, x_2)$ and $\exp[-(\frac{\varepsilon_{pk}}{F_0})^m]$ cannot be equal to zero, then Equation (13) can be simplified as:

$$1 - m(\frac{\varepsilon_{pk}}{F_0})^m = 0. \tag{14}$$

Equation (11) and Equation (14) are solved simultaneously, and then the unknown parameters m and F_0 can be obtained:

$$m = -\frac{1}{\ln\left\{\sigma_{pk} / [E(x_1,x_2)\varepsilon_{pk}]\right\}}, \tag{15}$$

$$F_0 = \frac{\varepsilon_{pk}}{\sqrt[m]{1/m}}. \tag{16}$$

Substituting Equation (15) and Equation (16) into Equation (10) gives:

$$\sigma = \begin{cases} E(x_1,x_2)\varepsilon \exp[-(\frac{\varepsilon \sqrt[m]{1/m}}{\varepsilon_{pk}})^m], \varepsilon < \varepsilon_m \\ E(x_1,x_2)\varepsilon_m \exp[-(\frac{\varepsilon_m \sqrt[m]{1/m}}{\varepsilon_{pk}})^m], \varepsilon \geq \varepsilon_m \end{cases} \tag{17}$$

UNIAXIAL COMPRESSION TESTS

Characteristics of the Tailings

The tailings used in this paper are from a copper mine located in northwest China, and the particle size distribution is shown in **Figure 2**. The average particle size d_{50} is 80.41 μm, the uniformity coefficient C_u is 8.57, and the curvature coefficient C_c is 1.71. As shown in **Figure 2**, the particle grading curve is smooth and continuous, and Fits grade is mild. Therefore, the tailings selected here have good gradation, compaction, and mechanical properties.

The chemical compositions of the tailings used in this paper are shown in **Figure 3**, which indicates that the main chemical compositions of the tailings are Fe_2O_3 and S_iO_2, accounting for 79% of the total solid weight. The content of CaO is less than 10%, which shows that the used tailings are low-calcium tailings.

Specimen Preparation and Experimental Equipment

CTB is composed of gelling agents, aggregates and water. The gelling agent used in this experiment is ordinary Portland cement P.O42.5, the aggregates are the tailings mentioned above and the water is ordinary city tap water from Xi'an in China's Shaanxi Province. Eight groups of CTB cylinder specimens with dimensions of 50 and 100 mm in diameter and height, respectively, were made to perform uniaxial compression tests. Three specimens were in each group, and a total of 24 specimens, contained five groups with a constant cement-sand ratio of 1/4 and solid contents of 70, 72, 74, 76, and 78 wt% and three groups with a constant solid content of 76 wt% and cement-sand ratios of 1/6, 1/8, and 1/10. The curing environment was set at a constant temperature of 20°C with a relative humidity of 95%, and the curing period was 28 days. Then, the average value of each group was taken as the final result for the relevant quantities.

The experimental equipment is LRT-300 electric-fluid servo triaxial compression machine (see **Figure 4**) and the sample is loaded as **Figure 5**. The loading process was controlled by displacement at the rate of 1×10^{-5} m/s.

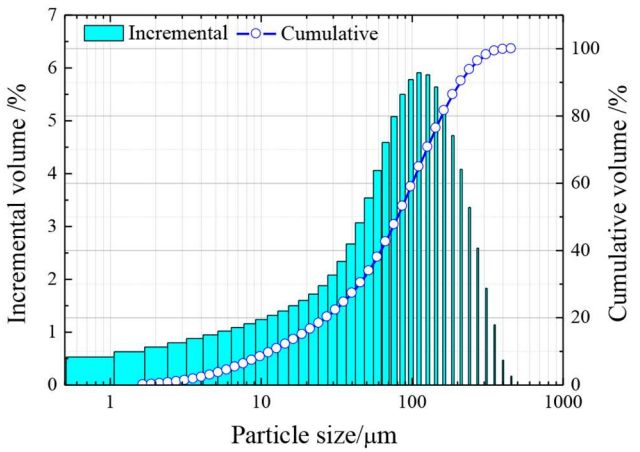

FIGURE 2 | Particle size distribution of the used tailings.

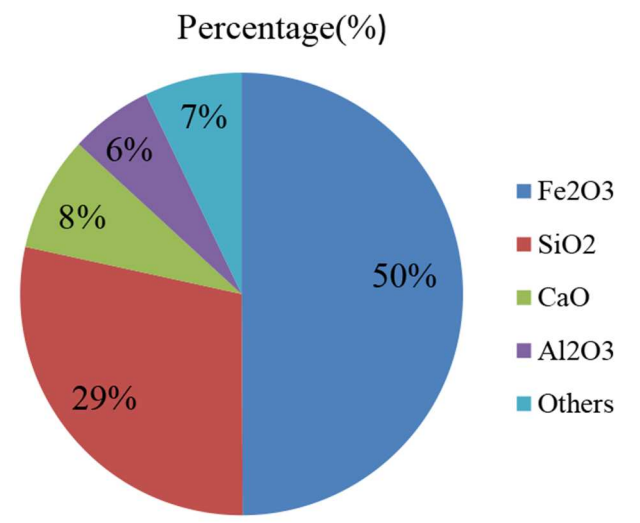

FIGURE 3 | Chemical components of the used tailings.

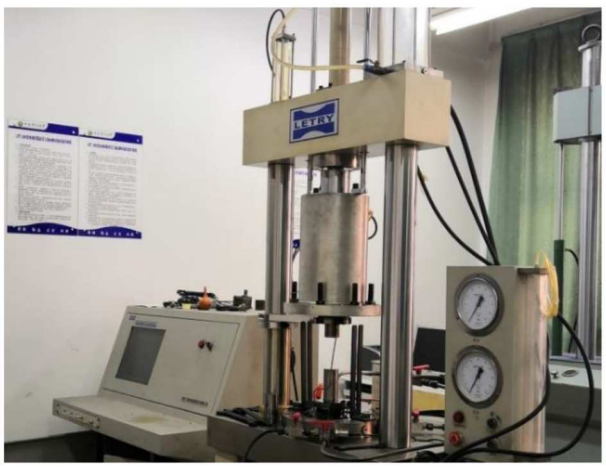

FIGURE 4 | LRT-300 electric-fluid servo triaxial compr-ession machine.

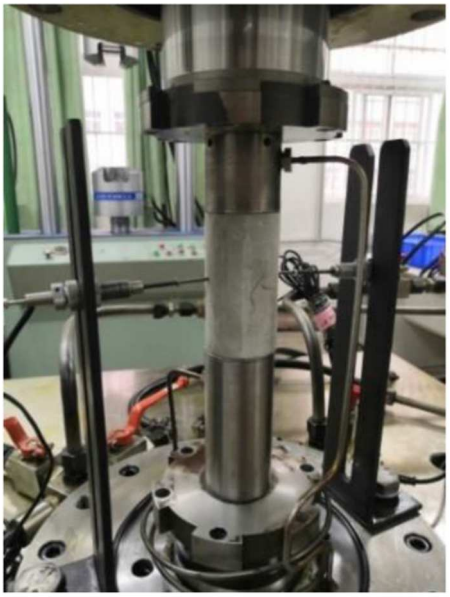

FIGURE 5 | Experimental process.

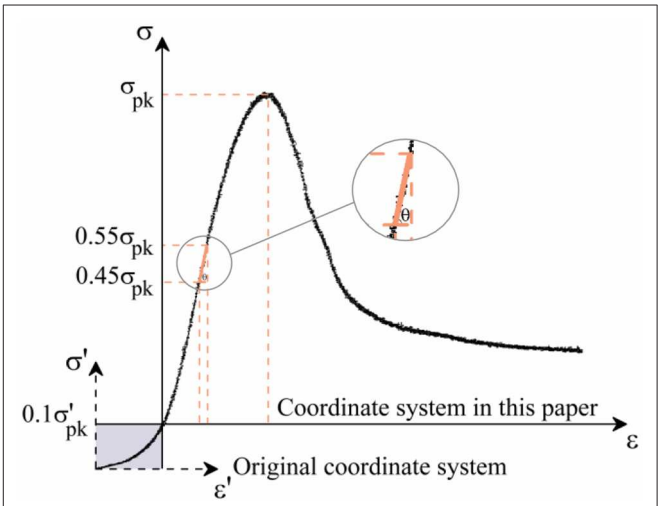

FIGURE 6 | Initial compaction stage and value of elastic modulus defined in this paper.

Model Parameters

Through experimental investigation, it is found that at the initial stage of loading, when the stress is less than 10% of the peak value, the CTB has a compaction phase, especially for the low strength specimens [51]. At this stage, the stress-strain curve is concave, and the initial cracks are closed under axial pressure. For convenience in application, the constitutive model is simplified into two stages in the theoretical part of this paper, without considering the initial compaction stage. Therefore, the initial compaction stage of the material is ignored in this paper, assuming that the material starts directly from the elastic stage after loading, as shown in **Figure 6**. σ'-ε' and σ'_{pk} represent the original coordinate system and the true peak stress, and σ-ε and

TABLE 1 | Model parameters and constitutive models.

Group number	Solid content /wt%	Cement-sand ratio	E /GPa	σ_{pk} /MPa	ε_{pk} /%	m	ε_m /%	Constitutive model ($\varepsilon < \varepsilon_m$)
1	70	1:4	0.74	3.80	0.74	2.74	1.60	$740\varepsilon \exp[-(93.54\varepsilon)^{2.74}]$
2	72	1:4	1.32	5.59	0.61	2.74	1.39	$1320\varepsilon \exp[-(113.48\varepsilon)^{2.74}]$
3	74	1:4	1.53	6.59	0.6	3.02	1.15	$1530\varepsilon \exp[-(115.58\varepsilon)^{3.02}]$
4	76	1:4	1.98	7.2	0.49	3.35	0.89	$1980\varepsilon \exp[-(142.26\varepsilon)^{3.35}]$
5	78	1:4	2.26	7.51	0.47	2.88	0.95	$2260\varepsilon \exp[-(147.37\varepsilon)^{2.88}]$
6	76	1:6	1.11	3.88	0.5	2.79	0.93	$1110\varepsilon \exp[-(138.46\varepsilon)^{2.79}]$
7	76	1:8	0.49	2.04	0.64	2.33	1.57	$490\varepsilon \exp[-(108.70\varepsilon)^{2.33}]$
8	76	1:10	0.21	1.37	0.78	5.60	1.33	$210\varepsilon \exp[-(94.25\varepsilon)^{5.60}]$

The parameters of each group in the table are the average values.

σ_{pk} represent the coordinate system selected in this paper and the corresponding peak stress, respectively.

The elastic modulus E is defined as the tangent of the secants corresponding to 45–55% of the peak stress [52]. The average stress-strain curve of the specimens with a cement-sand ratio of 1/4 and a solid content of 76 wt% was taken as an example to show the value of the elastic modulus E defined in this paper (see **Figure 6**).

Table 1 lists the values of σ_{pk} and the model parameters involved in the constitutive model of Equation (17). Meanwhile, the first stages of the corresponding constitutive models are given. The average stress-strain curve of the three CTB cylinder specimens for each group was obtained. Then, the variables of E, σ_{pk}, ε_{pk}, and ε_m in **Table 1** were gained from the average stress-strain curves. The value of E was defined as **Figure 6**, σ_{pk} and ε_{pk} are the peak stress and strain of the average curves, ε_m is the starting strain of the residual stage, and m was calculated according to Equation (15).

RESULTS AND DISCUSSION

Effects of Solid Content and Cement-Sand Ratio

Different solid contents (70, 72, 74, 76, and 78 wt%) and cement-sand ratios (1/4, 1/6, 1/8, and 1/10) were considered in the tests to analyze the effects of solid content and cement-sand ratio on the mechanical properties of CTB. The change in the mean stress-strain curves and the basic mechanical variables with solid contents and cement-sand ratios are shown in **Figures 7**, **8**. The values of all the relevant variables in each group are the mean values of the three specimens.

It can be seen from **Figure 7** that the solid content gradually increases from 70 to 78 wt% or the cement-sand ratio gradually increases from 1/10 to 1/4, the peak points of the stress-strain curves rise and shift to the left relative to the axis, which indicates that the strength (σ_{pk} and σ_m), the elastic modulus E and the energy dissipation capacity of the CTB specimens increases, while ε_{pk} decreases. Meanwhile, with the increase of the solid content or the cement-sand ratio, the descending part of the curves gradually steepens, which indicates that the ductility decreases and the friability increases.

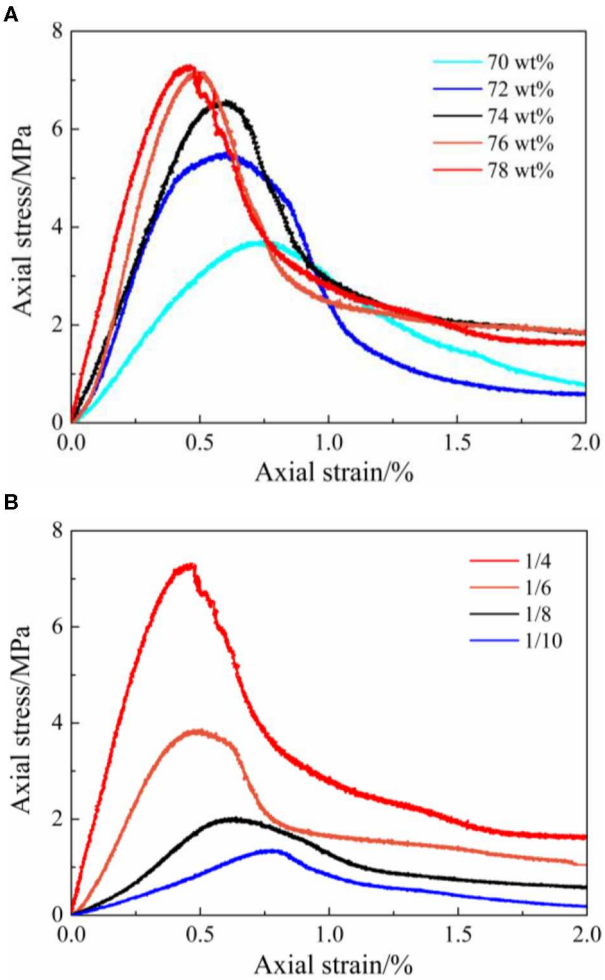

FIGURE 7 | Stress-strain curves for different solid contents and cement-sand ratios: **(A)** solid contents, **(B)** cement-sand ratios.

From **Figure 8A**, it can be observed that when the solid content ranges from 70 to 78 wt%, the corresponding value of E varies between 0.5 and 2.0 GPa, σ_{pk} varies between 4.0 and 7.5

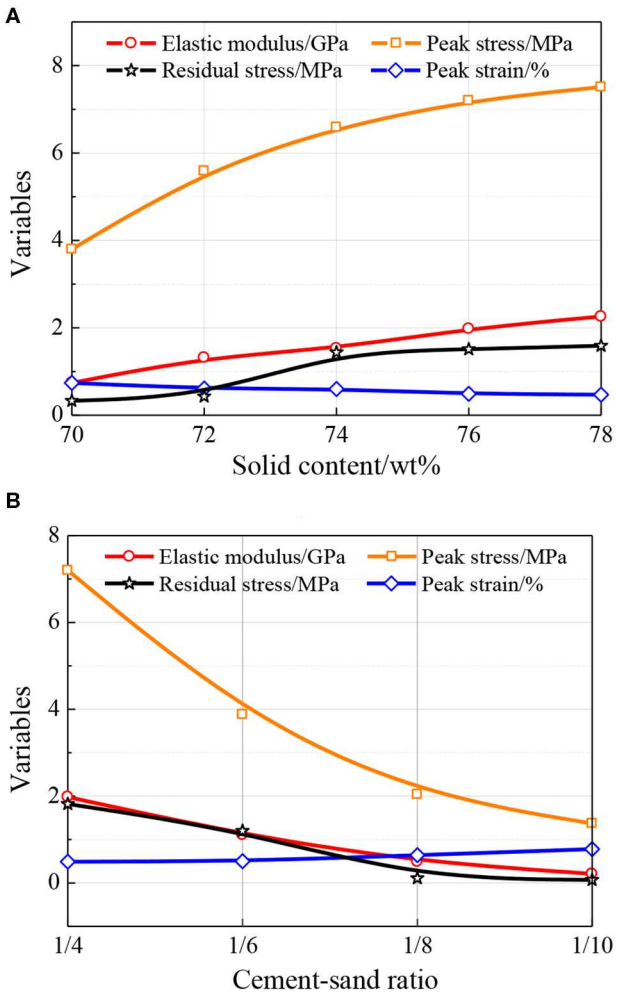

FIGURE 8 | Basic mechanical variables for different solid contents and cement-sand ratios: **(A)** solid contents, **(B)** cement-sand ratios.

MPa, ε_{pk} varies between 0.5 and 0.8% and σ_m varies between 0.5 and 1.5 MPa. Then, if the initial compaction stage is considered, the value range of σ_{pk} is from 4.5 to 8.5 MPa and the value range of σ_m is from 1.0 to 2.5 MPa.

From **Figure 8B**, it can be observed that when the cement-sand ratio ranges from 1/4 to 1/10, the corresponding value of E varies between 0.5 and 2.0 GPa, σ_{pk} varies between 1.5 and 7.5 MPa, ε_{pk} varies between 0.5 and 0.8% and σ_m varies between 1.0 and 2.0 MPa. Then, if the initial compaction stage is considered, the value range of σ_{pk} is from 2.0 to 8.5 MPa, and the value range of σ_m is form 0.3 to 3.0 MPa.

As shown in **Figure 8**, the influence of the solid content and cement-sand ratio on σ_{pk} is more obvious than that of the other quantities (E, ε_{pk} and σ_m), and the variation gradients of E and σ_m increase with the increase of solid content and cement-sand ratio are approximately equal. From **Figures 7**, **8**, it can be seen that the increasing gradient of σ_{pk} gradually decreases with the increase of solid content but increases with the increase of cement-sand ratio.

Verification and Comparison of the Constitutive Model

To verify the validity of the constitutive model of CTB established in this paper, the experimental results are compared with those calculated using the theoretical model. The calculated and experimental results are in good agreement, especially in the pre-peak region (see **Figure 9**). Therefore, the proposed constitutive model can be used to describe the mechanical properties of CTB under uniaxial compression.

Ordinary cement mortar is also composed of gelling agents, aggregates and water, which is similar to the composition of CTB except that the aggregates are river sand and not tailings. To compare and illustrate the performance difference between the two materials under uniaxial compression, the peak point of the stress-strain curves for ordinary cement mortar M5 in reference [53] was scaled by the average peak value of each group of specimens in this paper. Then, the uniaxial compression stress-strain curves of the CTB and ordinary cement mortar M5 are compared in **Figure 9**. It can be seen that before the residual stress, the curves of the two materials are similar in shape. However, the CTB exhibits obvious residual stress, but the ordinary cement mortar M5 does not. Furthermore, the ordinary cement mortar M5 is slightly stronger than CTB at the pre-failure stage, but slightly weaker at the post-failure stage.

Meanwhile, it can also be seen from **Figure 9** that under uniaxial compression, the CTB cylinder specimens are subjected to axial compression and transverse tension. The major failure mode is columnar splitting failure caused by tensile stress.

Limitations and Future Work

The results of the two-stage constitutive model for CTB proposed in this paper is in good agreement with the experimental results and can be used to predict the constitutive relation of CTB under uniaxial compression. The constitute model provided here is generally applicable, but the model parameters need to be specifically determined by testing the tailings from different sources.

Meanwhile, the long-term stress state of the CTB is constrained in three directions rather than in one direction. Therefore, our future work will investigate the mechanical properties of CTB under triaxial compression by triaxial compression tests and provide a simple and universally applicable triaxial compression constitutive model.

CONCLUSIONS

In this paper, the constitutive model for low-calcium copper mine tailings under uniaxial compression has been studied. The validity of the proposed two-stage constitutive model for CTB was verified by a comparison with the test results. Meanwhile, the effects of solid content and cement-sand ratio on the mechanical properties of CTB were also analyzed. The results are described as follows:

i) With the increase of solid content or cement-sand ratio, the strength (σ_{pk} and σ_m), E and energy dissipation capacity of

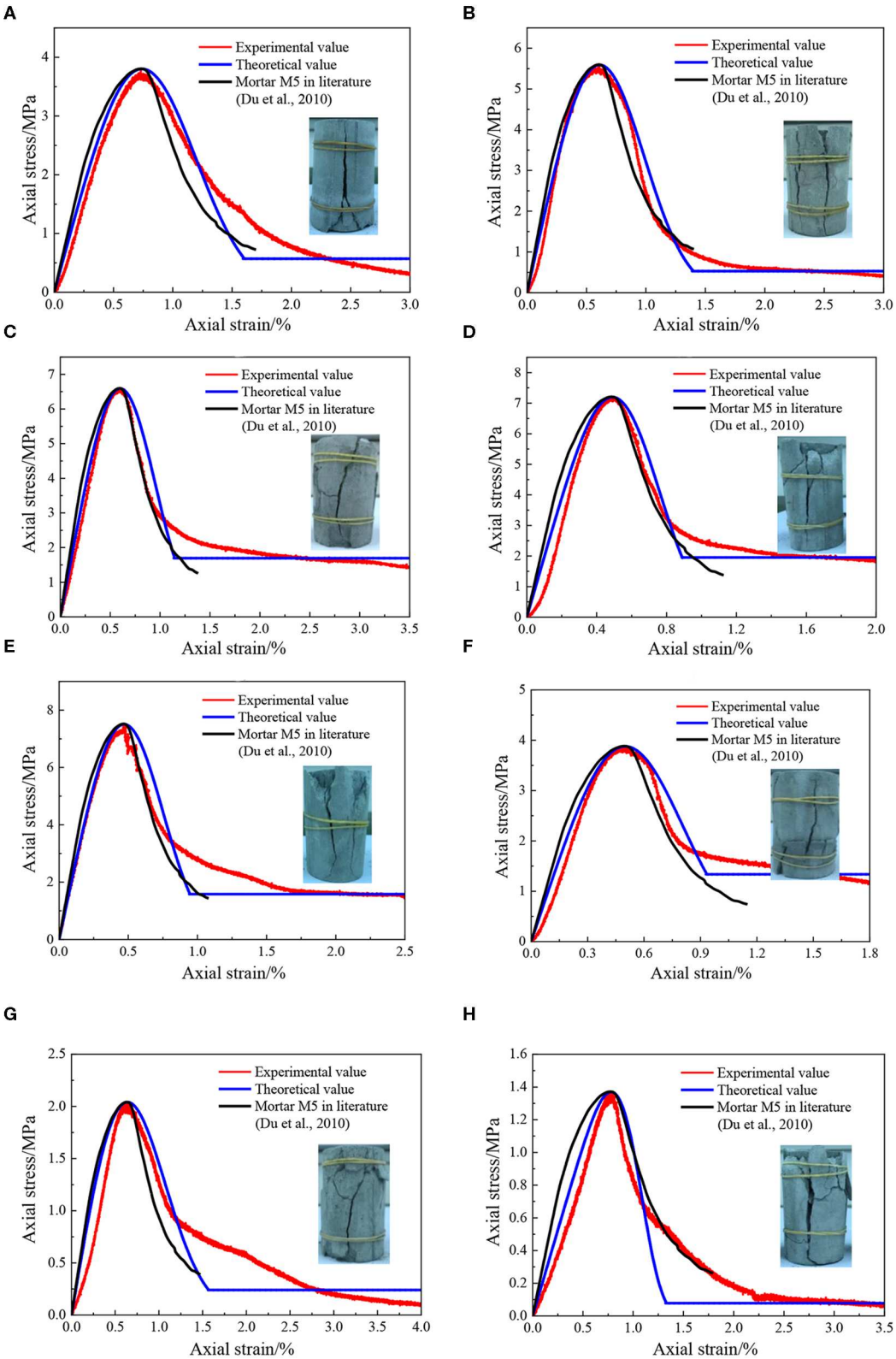

FIGURE 9 | Comparison of theoretical and experimental results for stress-strain curves (cement-sand ratio = C/S, solid content = SC): **(A)** C/S = 1/4 and SC = 70 wt%, **(B)** C/S = 1/4 and SC = 72 wt%, **(C)** C/S = 1/4 and SC = 74 wt%, (**D**) C/S = 1/4 and SC = 76 wt%, **(E)** C/S = 1/4 and SC = 78 wt%, **(F)** C/S = 1/6 and SC = 76 wt%, **(G)** C/S = 1/8 and SC = 76 wt%, **(H)** C/S = 1/10 and SC = 76 wt%.

the CTB increased, but ε_{pk} and the ductility decreased. The influence on σ_{pk} is more obvious than that on the other quantities (E, ε_{pk} and σ_m).

ii) Regardless of the initial compaction stage, for CTB specimens with solid contents of 70–78 wt% and cement-sand ratios of 1/4–1/10, the corresponding value of E remained between 0.5 and 2.0 GPa, σ_{pk} remained between 1.5 and 7.5 MPa, ε_{pk} remained between 0.5 and 0.8% and σ_m remained between 0.5 and 2.0 MPa. Then, if the initial compaction stage was considered, σ_{pk} ranged from 2.0 to 8.5 MPa and σ_m ranged from 0.3 to 3.0 MPa.

iii) The stress-strain curve of CTB is similar to that of ordinary cement mortar M5 but exhibits obvious residual stress. The failure mode of the CTB samples under uniaxial compression is mainly columnar splitting failure caused by tensile stress.

DATA AVAILABILITY STATEMENT

The raw data supporting the conclusions of this article will be made available by the authors, without undue reservation, to any qualified researcher.

AUTHOR CONTRIBUTIONS

BT and KC: writing-original draft preparation. LL: conceptualization. BZ: methodology. YZ: data curation. KS: validation. QY: supervision. All authors have read and agreed to the published version of the manuscript.

FUNDING

This research was supported by the National Natural Science Foundation of China (Nos. 51674188, 51874229, 51504182, 51974225, 51904224, 51904225, and 51704229), Shaanxi Innovative Talents Cultivate Program-New-star Plan of Science and Technology (No. 2018KJXX-083), Natural Science Basic Research Plan of Shaanxi Province of China (Nos. 2018JM5161, 2018JQ5183, 2015JQ5187, and 2019JM-074), Scientific Research Program funded by the Shaanxi Provincial Education Department (Nos. 2019JQ-354, 15JK1466, and 19JK0543), China Postdoctoral Science Foundation (No. 2015M582685), Open Project of State Key Laboratory of Green Building in Western China (No. LSKF201915), and Outstanding Youth Science Fund of Xi'an University of Science and Technology (No. 2018YQ2-01).

ACKNOWLEDGMENTS

The authors are grateful for the support provided by College of Science and Energy School, Xi'an University of Science and Technology, Xi'an, 710054, China.

REFERENCES

1. Dong L, Sun D, Shu W, Li X. Exploration: safe and clean mining on Earth and asteroids. *J Clean Prod.* (2020) **257**:120899. doi: 10.1016/j.jclepro.2020.120899
2. Sun X, Wang W. Theoretical research on high water material replacement mining the strip coal pillar above confined aquifer. *J China Coal Soc.* (2011) **36**:909–13. doi: 10.13225/j.cnki.jccs.2011.06.018
3. Zhang Q, Zhang J, Huang Y, Ju F. Backfilling technology and strata behaviors in fully mechanized coal mining working face. *Int J Mining Sci. Technol.* (2012) **22**:151–7. doi: 10.1016/j.ijmst.2011.08.003
4. Yilmaz E, Belem T, Bussiere B, Mbonimpa M, Benzaazoua M. Curing time effect on consolidation behaviour of cemented paste backfill containing different cement types and contents. *Constr Build Mater.* (2015) **75**:99–111. doi: 10.1016/j.conbuildmat.2014.11.008
5. Belem T, Benzaazoua M. Design and application of underground mine paste backfill technology. *Geotech Geol Eng.* (2007) **26**:147–74. doi: 10.1007/s10706-007-9154-3
6. Qi C, Chen Q, Fourie A, Zhang Q. An intelligent modelling framework for mechanical properties of cemented paste backfill. *Miner Eng.* (2018) **123**:16–27. doi: 10.1016/j.mineng.2018.04.010
7. Kesimal A, Yilmaz E, Ercikdi B, Alp I, Deveci H. Effect of properties of tailings and binder on the short-and long-term strength and stability of cemented paste backfill. *Mater Lett.* (2005) **59**:3703–9. doi: 10.1016/j.matlet.2005.06.042
8. Ercikdi B, Cihangir F, Kesimal A, Deveci H, Alp I. Utilization of water-reducing admixtures in cemented paste backfill of sulphide-rich mill tailings. *J Hazard Mater.* (2010) **179**:940–6. doi: 10.1016/j.jhazmat.2010.03.096
9. Cihangir F, Ercikdi B, Kesimal A, Deveci H, Erdemir F. Paste backfill of high-sulphide mill tailings using alkali-activated blast furnace slag: effect of activator nature, concentration and slag properties. *Miner Eng.* (2015) **83**:117–27. doi: 10.1016/j.mineng.2015.08.022
10. Chen Q, Zhang Q, Qi C, Fourie A, Xiao C. Recycling phosphogypsum and construction demolition waste for cemented paste backfill and its environmental impact. *J Clean Prod.* (2018) **186**:418–29. doi: 10.1016/j.jclepro.2018.03.131
11. Liu L, Fang Z, Qi C, Zhang B, Guo L, Song K. Experimental investigation on the relationship between pore characteristics and unconfined compressive strength of cemented paste backfill. *Constr Build Mater.* (2018) **179**:254–64. doi: 10.1016/j.conbuildmat.2018.05.224
12. Lu H, Qi C, Chen Q, Chen Q, Gan D, Xue Z, et al. A new procedure for recycling waste tailings as cemented paste backfill to underground stopes and open pits. *J Clean Prod.* (2018) **188**:601–12. doi: 10.1016/j.jclepro.2018.04.041
13. Cao S, Song W. Effect of filling interval time on long-term mechanical strength of layered cemented tailing backfill. *Adv Mater Sci Eng.* (2016) **2016**:1–7. doi: 10.1155/2016/9507852
14. Cao S, Song W. Effect of filling interval time on the mechanical strength and ultrasonic properties of cemented coarse tailing backfill. *Int J Miner Process.* (2017) **166**:62–8. doi: 10.1016/j.minpro.2017.07.005
15. Cao S, Song W, Yilmaz E. Influence of structural factors on uniaxial compressive strength of cemented tailings backfill. *Constr Build Mater.* (2018) **174**:190–201. doi: 10.1016/j.conbuildmat.2018.04.126
16. Jiang H, Fall M. Yield stress and strength of saline cemented tailings in sub-zero environments: Portland cement paste backfill. *Int J Min Process.* (2017) **160**:68–75. doi: 10.1016/j.minpro.2017.01.010
17. Yin S, Shao Y, Wu A, Wang Y, Chen X. Expansion and strength properties of cemented backfill using sulphidic mill tailings. *Constr Build Mater.* (2018) **165**:138–48. doi: 10.1016/j.conbuildmat.2018.01.005
18. Zheng J, Guo L, Sun X, Li W, Jia Q. Study on the strength development of cemented backfill body from lead-zinc mine tailings with sulphide. *Adv Mater Sci Eng.* (2018) **2018**:1–8. doi: 10.1155/2018/7278014
19. Xu W, Li Q, Zhang Y. Influence of temperature on compressive strength, microstructure properties and failure pattern of fiber-reinforced cemented tailings backfill. *Constr Build Mater.* (2019) **222**:776–85. doi: 10.1016/j.conbuildmat.2019.06.203
20. Zheng J, Zhu Y, Zhao Z. Utilization of limestone powder and water-reducing admixture in cemented paste backfill of coarse copper mine tailings.

Constr Build Mater. (2016) **124**:31–6. doi: 10.1016/j.conbuildmat.2016.07.055
21. Hou C, Zhu W, Yan B, Guan K, Du J. Influence of binder content on temperature and internal strain evolution of early age cemented tailings backfill. *Constr Build Mater.* (2018) **189**:585–93. doi: 10.1016/j.conbuildmat.2018.09.032
22. Mangane M, Argane R, Trauchessec R, Lecomte A, Benzaazoua M. Influence of superplasticizers on mechanical properties and workability of cemented paste backfill. *Miner Eng.* (2018) **116**:3–14. doi: 10.1016/j.mineng.2017.11.006
23. Zheng J, Sun X, Guo L, Zhang S, Chen J. Strength and hydration products of cemented paste backfill from sulphide-rich tailings using reactive MgO-activated slag as a binder. *Constr Build Mater.* (2019) **203**:111–9. doi: 10.1016/j.conbuildmat.2019.01.047
24. Xu W, Cao P, Tian M. Strength development and microstructure evolution of cemented tailings backfill containing different binder types and contents. *Minerals.* **8**:167. doi: 10.3390/min8040167
25. Liu L, Xin J, Feng Y, Zhang B, Song K. Effect of the cement-tailing ratio on the hydration products and microstructure characteristics of cemented paste backfill. *Arab J Sci Eng.* (2019) **44**:6547–56. doi: 10.1007/s13369-019-03954-z
26. Xu W, Cao Y, Liu B. Strength efficiency evaluation of cemented tailings backfill with different stratified structures. *Eng Struct.* (2019) **180**:18–28. doi: 10.1016/j.engstruct.2018.11.030
27. Jiang H, Fall M, Cui L. Freezing behaviour of cemented paste backfill material in column experiments. *Constr Build Mater.* (2017) **147**:837–46. doi: 10.1016/j.conbuildmat.2017.05.002
28. Yi X, Ma G, Fourie A. Compressive behaviour of fibre-reinforced cemented paste backfill. *Geotext Geomembr.* (2015) **43**:207–15. doi: 10.1016/j.geotexmem.2015.03.003
29. Chen X, Shi X, Zhou J, Chen Q, Li E, Du X. Compressive behavior and microstructural properties of tailings polypropylene fibre-reinforced cemented paste backfill. *Constr Build Mater.* (2018) **190**:211–21. doi: 10.1016/j.conbuildmat.2018.09.092
30. Cao S, Yilmaz E, Song W. Fiber type effect on strength, toughness and microstructure of early age cemented tailings backfill. *Constr Build Mater.* (2019) **223**:44–54. doi: 10.1016/j.conbuildmat.2019.06.221
31. Xue G, Yilmaz E, Song W, Yilmaz E. Influence of fiber reinforcement on mechanical behavior and microstructural properties of cemented tailings backfill. *Constr Build Mater.* (2019) **213**:275–85. doi: 10.1016/j.conbuildmat.2019.04.080
32. Wang M, Liu L, Wang S, Lv B, Zhang B, Zhang X, et al. Numerical investigation of heat transfer and phase change characteristics of cold load and storage functional CPB in deep mine. *Front Earth Sci.* (2020) **8**:31. doi: 10.3389/feart.2020.00031
33. Hu J, Ren Q, Jiang Q, Gao R, Zhang L, Luo Z. Strength characteristics and the reaction mechanism of stone powder cement tailings backfill. *Adv Mater Sci Eng.* (2018) **2018**:1–14. doi: 10.1155/2018/8651239
34. Cao S, Yilmaz E, Song W, Yilmaz E, Xue G. Loading rate effect on uniaxial compressive strength behavior and acoustic emission properties of cemented tailings backfill. *Constr Build Mater.* (2019) **213**:313–24. doi: 10.1016/j.conbuildmat.2019.04.082
35. Sun Q, Cai C, Zhang S, Tian S, Li B, Xia Y, et al. Study of localized deformation in geopolymer cemented coal gangue-fly ash backfill based on the digital speckle correlation method. *Constr Build Mater.* (2019) **215**:321–31. doi: 10.1016/j.conbuildmat.2019.04.208
36. Wang Y, Wu A, Wang H, Wang Y, Cui L, Jin F, et al. Damage constitutive model of cemented tailing paste under initial temperature effect. *Chinese J Eng.* (2017) **39**:31–8. doi: 10.13374/j.issn2095-9389.2017.01.004
37. Cui L, Fall M. A coupled thermo–hydro-mechanical–chemical model for underground cemented tailings backfill. *Tunnel Undergr Space Technol.* (2015) **50**:396–414. doi: 10.1016/j.tust.2015.08.014
38. Wu D, Deng T, Zhao R. A coupled THMC modeling application of cemented coal gangue-fly ash backfill. *Constr Build Mater.* (2018) **158**:326–36. doi: 10.1016/j.conbuildmat.2017.10.009
39. Cui L, Fall M. An evolutive elasto-plastic model for cemented paste backfill. *Comput Geotech.* (2016) **71**:19–29. doi: 10.1016/j.compgeo.2015.08.013
40. Qi C, Fourie A, Chen Q, Zhang Q. A strength prediction model using artificial intelligence for recycling waste tailings as cemented paste backfill. *J Clean Prod.* (2018) **183**:566–78. doi: 10.1016/j.jclepro.2018.02.154
41. Qi C, Chen Q, Fourie A, Tang X, Zhang Q, Dong X, et al. Constitutive modelling of cemented paste backfill: a data-mining approach. *Constr Build Mater.* (2019) **197**:262–70. doi: 10.1016/j.conbuildmat.2018.11.142
42. Qi C, Tang X, Dong X, Chen Q, Fourie A, Liu E. Towards Intelligent Mining for Backfill: a genetic programming-based method for strength forecasting of cemented paste backfill. *Miner Eng.* (2019) **133**:69–79. doi: 10.1016/j.mineng.2019.01.004
43. Wu E. *Specific energy characteristics of cemented tailings backfill of damage and fracture under uniaxial compression* (Master). Wuhan: Wuhan University of Science and Technology (2018).
44. Dong L, Tong X, Li X, Zhou J, Wang S, Liu B. Some developments and new insights of environmental problems and deep mining strategy for cleaner production in mines. *J Clean Prod.* (2019) **210**:1562–78. doi: 10.1016/j.jclepro.2018.10.291
45. Wang J, Song W, Tan Y, Fu J, Cao S. Damage constitutive model and strength criterion of horizontal stratified cemented backfill. *Rock Soil Mech.* (2019) **40**:1731–9. doi: 10.16285/j.rsm.2018.0017
46. Ahmad A, Ghazal M. Exponentiated additive Weibull distribution. *Reliabil Eng Syst Saf.* (2020) **193**:106663. doi: 10.1016/j.ress.2019.106663
47. Zhang H, Yuan C, Yang G, Wu LY, Peng C, Ye W, Shen Y, Moayedi H. A novel constitutive modelling approach measured under simulated freeze–thaw cycles for the rock failure. *Eng. Comput.* (2019) 35:1–14. doi: 10.1007/s00366-019-00856-4
48. Dong L, Sun D, Li X, Ma J, Zhang L, Tong X. Interval non-probabilistic reliability of surrounding jointed rockmass considering microseismic loads in mining tunnels. *Tunnel Undergr Space Technol.* (2018) **81**:326–35. doi: 10.1016/j.tust.2018.06.034
49. Lemaitre J. A continuous damage mechanics model for ductile fracture. *J Eng Mater Technol.* (1985) **107**:83–9. doi: 10.1115/1.3225775
50. Dong L, Shu W, Li X, Zhang J. Quantitative evaluation and case studies of cleaner mining with multiple indexes considering uncertainty factors for phosphorus mines. *J Clean Prod.* (2018) **183**:319–34. doi: 10.1016/j.jclepro.2018.02.105
51. Cheng A, Zhang Y, Dai S, Dong F, Zeng W, Li D. Space-time evolution of acoustic emission parameters of cemented backfill and its fracture prediction under uniaxial compression. *Rock Soil Mech.* (2019) **40**:2965–74. doi: 10.16285/j.rsm.2018.1940
52. Wang X, Kang H, Gao F, Zhao K. DEM simulation of mechanical behavior of jointed coal in large scale under uniaxial compression. *J China Coal Soc.* (2018) **43**:3088–97. doi: 10.13225/j.cnki.jccs.2018.0834
53. Du X, Wang Y, Lu D. Study on static and dynamic stress strain relationship of cement mortar material. *China Civil Eng J.* (2010) **43S**:119–26. doi: 10.15951/j.tmgcxb.2010.s2.033

Conflict of Interest: The authors declare that the research was conducted in the absence of any commercial or financial relationships that could be construed as a potential conflict of interest.